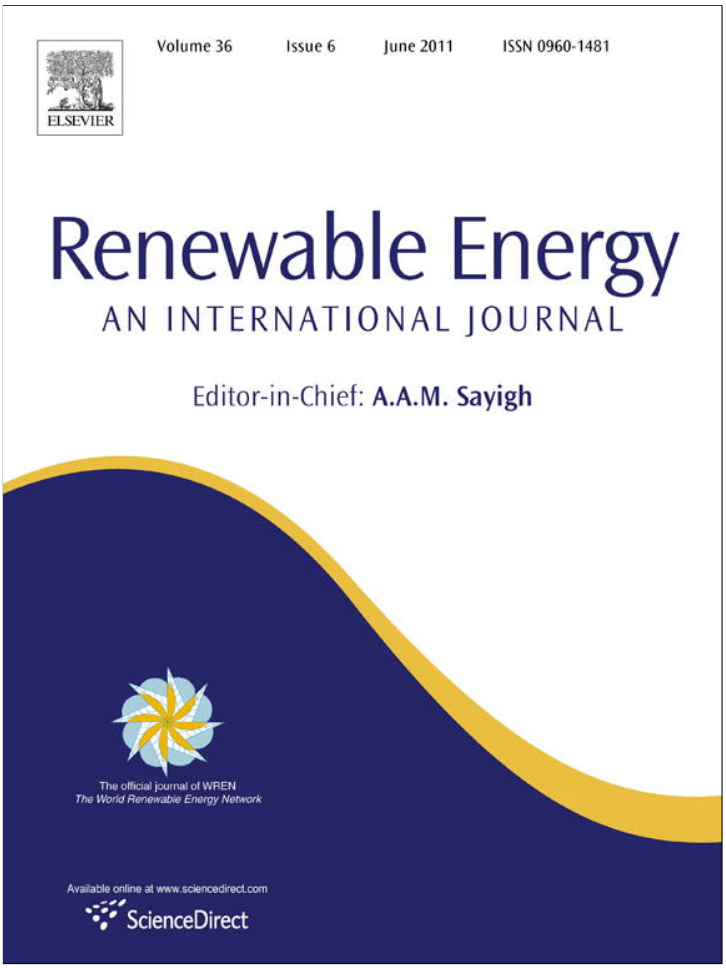

Renewable Energy 36 (2011) 1788–1794

Contents lists available at ScienceDirect

Renewable Energy

journal homepage: www.elsevier.com/locate/renene

High performance high-purity sol-gel derived carbon supercapacitors from renewable sources

Betzaida Batalla Garcia, Stephanie L. Candelaria, Dawei Liu, Saghar Sepheri, James A. Cruz, Guozhong Cao*

University of Washington, Department of Materials Science and Engineering, 302 Roberts Hall, Seattle, WA 98195-2120, United States

ARTICLE INFO

Article history:
Received 13 August 2010
Accepted 27 November 2010
Available online 21 December 2010

Keywords:
Sol-gel
Porous material
Carbon cryogel
Impedance spectroscopy

ABSTRACT

In this study highly pure carbons synthesized using resorcinol furaldehyde catalyzed with hexamethylenetetramine (an amine base) are tested for supercapacitor electrodes. This synthesis is not only from all-organic renewable sources, but can also significantly increase the performance of the device by promoting adequate electric double layer formation. The electrochemical characterization shows an increase in the specific capacitance per unit of surface area that is 18% higher than that of commercial biomass carbons and their synthetic counterparts. The life of the capacitor is also extended to twice that of the commercial brand tested here and has increased power after cycling. The supercapacitors made from this synthesis have electric double layer characteristics as desired in some applications. The samples have been tested for composition using XPS, and their electrochemical performance was analyzed using galvanostatic measurements and complex capacitance and power derived from impedance spectroscopy.

1. Introduction

Energy storage is receiving more attention as the focus shifts away from fossil fuels and towards renewable energy generation. Because of the intermittent nature of wind, solar, and other renewable energy resources, devices such as batteries and supercapacitors play a role in making these new technologies viable. Energy can be collected and stored during peak generation times, then recovered in order to meet demand during off-peak hours [1]. Ideally, an energy storage device used for this sort of application would be able to withstand intensive cycling so that it only needs to be replaced periodically.

Carbon electric double layer supercapacitors (EDLSC) are the only currently commercialized supercapacitors that have cyclic stabilities exceeding millions of cycles. In contrast, pseudocapacitors, like batteries, are still within the 100,000 cycle range [2]. Currently, EDLSC have benefited from a wide variety of precursors taken from renewable resources, including both biomass and its derivatives. Because biomass naturally contains ash, the tendency in recent studies has been to promote faradaic reactions from the ash as a means to utilize these impurities [3,4]. Although the faradaic reactions are useful in aqueous electrolyte systems, their effect on the organic electrolytes used for EDLSC can be detrimental in some cases [5,6].

Organic electrolytes have several advantages over aqueous electrolytes. They can be used at high voltages exceeding 2 V, they have long cyclic stability, and they are resistant to high temperature. This is possible because EDLSC rely on an electrostatic mechanism, the formation of the electrical double layer, to store charge and deliver power. Unfortunately, organic electrolytes can be susceptible to faradaic reactions that can reduce the performance of the device, as will be shown in this study. Examples of detrimental effects are the self-discharge of the capacitor due to iron impurities and oxidation of the electrolyte during charge–discharge cycles [5]. Therefore, to promote the formation of an optimal electric double layer, impurities must be eliminated.

However, biomass can also be the source of highly pure carbon precursors with the high surface area needed to promote and maintain electric double layer formation. In addition, the use of fine renewable precursors from biomass can potentially reduce the amount of harmful chemicals used during synthesis, and simplify the post processing. To understand the role of biomass and its derivatives in the production of EDLSC, some knowledge about the synthesis of the electrodes is necessary.

Carbon electrodes for supercapacitors are produced using various processing techniques, starting with an available organic source like wood or a derivative such as phenolic resins. This source is dried, pyrolyzed, and then activated to increase the surface area and open the pore structure. Woody biomass, and other plant matter like seaweed, nuts, etc., is usually pyrolyzed in an inert atmosphere to carbonize the material. However, post treatments to

* Corresponding author. Tel.: +1 206 6169084; fax: +1 206 5433100.
E-mail address: gzcao@u.washington.edu (G. Cao).

0960-1481/$ – see front matter © 2010 Elsevier Ltd. All rights reserved.
doi:10.1016/j.renene.2010.11.030

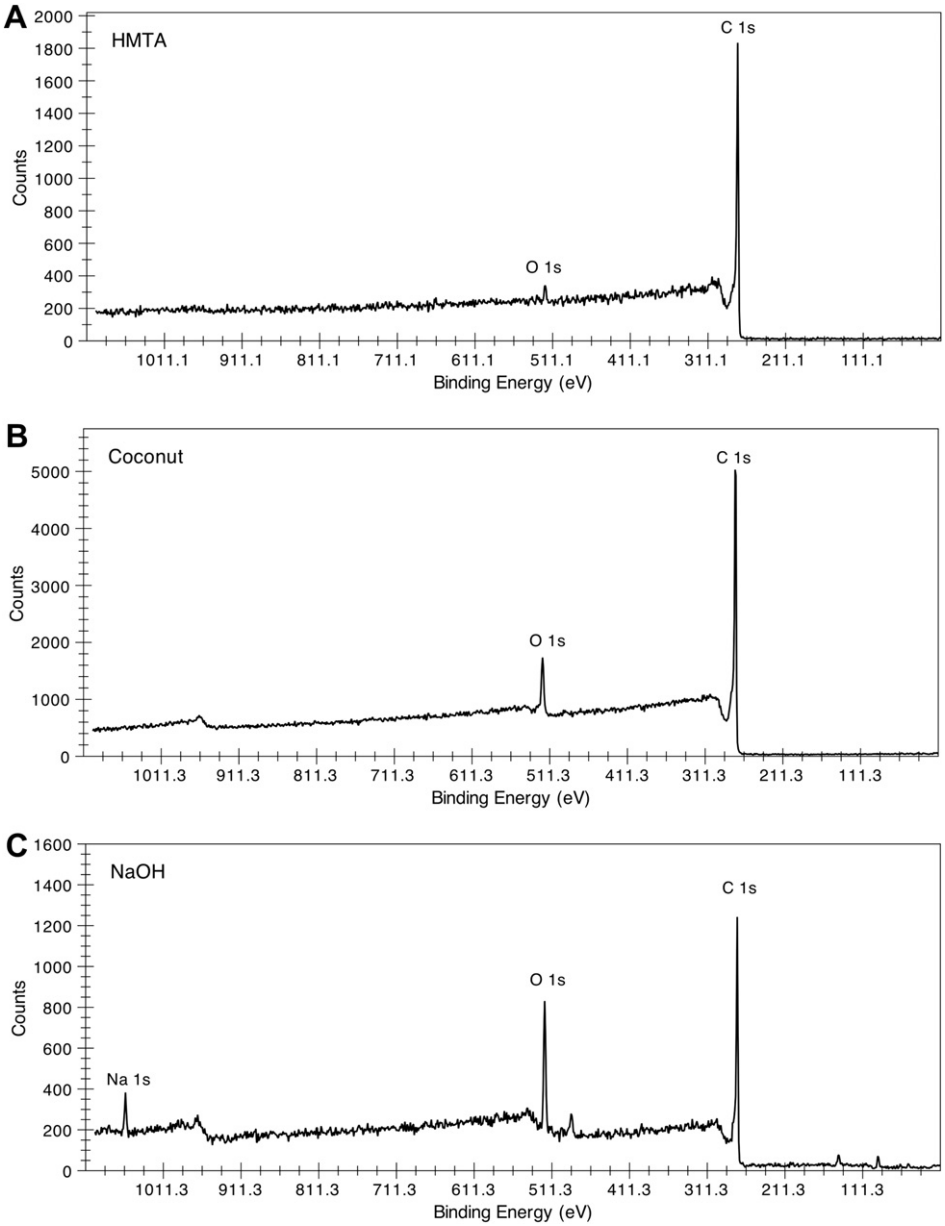

Fig. 1. XPS spectra of sample catalyzed using HMTA (A), commercial sample YP17 from coconut shells (B), and sample catalyzed using NaOH (C).

reduce the ash content are necessary when high purity is required. Additionally, CO_2, ZnCl, KOH salts, and HCl are commonly used to activate the carbon [3,4,7]. Although no intensive processing is required to obtain the raw material, post processing is required to remove the salts, which is then followed by various subsequent drying steps. Even so, substantial amounts of impurities can be left in the final product. Additionally, because biomass is a natural product, there is limited control over the pore structure and chemical composition of the final product.

On the other hand, synthetic phenolic carbons, such as aerogels and cryogels, have advantages over biomass in that the pore size distribution can be tuned to a specific electrolyte ion, and chemical composition can be controlled. These phenolic carbons, which are synthesized using aqueous solutions and metal ion catalysts, provide the opportunity to tune the pore structure. However, they require repeated solvent exchanges to both neutralize the catalyst and reduce the capillary forces that occur during specialized drying processes (like freeze drying and supercritical drying) in order to preserve the pore structure. Pyrolysis in N_2 and activation in CO_2, air, or steam are common procedures to increase the surface area. The post processing described here can be costly and unfortunately leave metal ion impurities that can later reduce the performance of the capacitor.

High purity carbons can be produced using precursors from all organic renewable sources like phenols, aldehydes, amines, starches, and sugars [8–11]. Due to the demand to decrease petroleum usage, there is an increased interest in producing fine

Table 1
Compositional data from XPS.

Sample ID	C	O	Na	Si
	Atomic %			
HMTA	98.2	1.8	–	–
YP17	92.1	7.8	–	–
NaOH	77.1	16.7	2.0	4.2

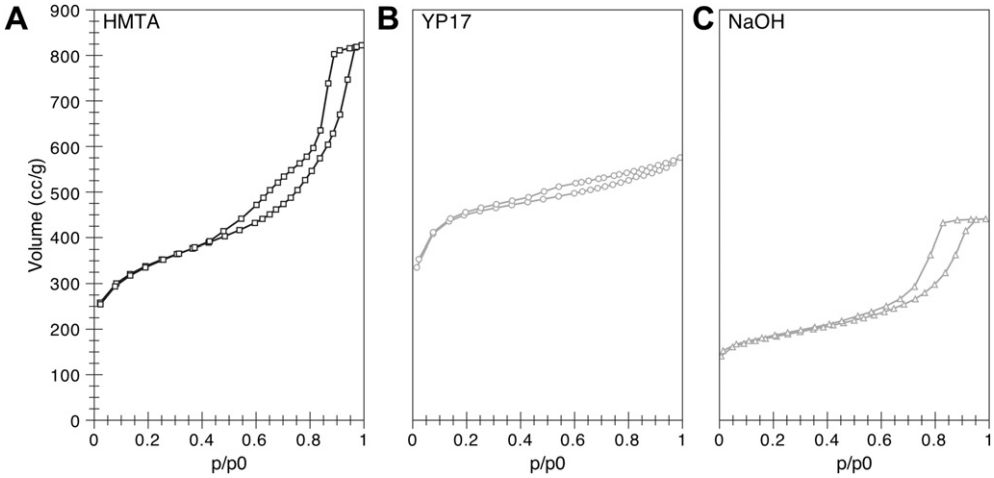

Fig. 2. Nitrogen physisorption isotherms for carbons prepared using HMTA (A), coconut shells (B), and NaOH (C).

chemicals with all-renewable synthesis [11,12], and among these chemicals are phenolic resins [12] such as resorcinol furaldehyde resins (RFF). Resorcinol and furaldehyde are synthesized from renewable plant sources like Brazil wood and sugarcane bagasse [13,14]. In addition, the catalyst used in this study, hexamethylenetetramine or HMTA, can be synthesized from formaldehyde and ammonia, which are also by-products of biomass.

These RFF gels catalyzed using hexametylenetetramine (HMTA) have been used for hydrogen storage [8]. More recently, our group studied the chemical composition of RFF gels catalyzed with HMTA, with pore structure optimization for supercapacitors and energy storage applications [9]. The findings reveal that HMTA not only tunes the pore size as a catalyst but also modifies the porosity by adding functional groups such as iminos to the colloidal structure. This RFF synthesis has the advantage that it can produce carbons with little or no metal ion impurities, which are otherwise responsible for the pseudocapacitive behavior that shortens the device life. The RFF synthesis also has advantages over other methods, such as the elimination of solvent exchange steps. This is due to the structural changes produced by the amine catalyst, which create high surface area carbons that can be air dried by the addition of the aforementioned functional groups [8,9]. Although refinement of the RFF precursors might have the energy and cost expenditure of producing such chemicals as a downside, the benefits must be measured against improvements in the performance of the resulting product. Note that evaluations of this nature are best addressed by a life cycle assessment [15] and are not relevant to this publication.

In this manuscript, resorcinol furaldehyde carbon cryogel electrodes are synthesized and tested against two other supercapacitor sources: metal ion catalyzed carbon cryogels and a commercial sample prepared using coconut shells (referred to as YP17). Their performance and chemical and electrochemical properties are characterized, and impedance spectroscopy is used to closely examine the complex energy and power losses.

2. Experimental

2.1. Synthesis and carbon electrodes

Samples were prepared using a process similar to that reported by Wu et al. [7], with resorcinol and furaldehyde as the precursors and either NaOH or HMTA as the catalyst. However, the polycondensation reaction took place in solvent mixtures. The furaldehyde to resorcinol (FR) molar ratio was set to 2.5 and the resorcinol to HMTA (RH) or NaOH molar ratio was 50. The resorcinol, furaldehyde, and HMTA were purchased from Sigma Aldrich. The samples were gelled for 7 days then freeze dried under vacuum at −50 °C in a Labconco FreeZone 1 L Freeze dryer. Pyrolysis was performed under N_2 at a ramp rate of 5 °C/min to a maximum temperature of 900 °C, where it was held for 180 min. Activation was performed in dried air at a ramp rate of 5 °C/min to a temperature of 420 °C, held for 240 min at this temperature, then re-pyrolyzed at the same ramp rate in N_2 for 180 min at 900 °C to remove any additional functional groups from the carbon. Thermogravimetric analysis was used to determine the activation level of the HMTA catalyzed samples.

2.2. Surface area and compositional analysis

The nitrogen sorption was performed using a Quantachrome NOVA 4200e. The total surface area (SA) was determined using the multipoint Brunauer Emmett Teller (BET) method. The Dubinin-Astakhov (DA) method was used to determine the micropore size distribution, a limiting factor in the electrolyte penetration.

All XPS spectra were taken on a Surface Science Instruments S-probe spectrometer. This instrument has a monochromatized Al X-ray source and a low energy electron flood gun for charge neutralization. X-ray spot size for these acquisitions was 800 × 800 μm. All samples were run as insulators meaning that charge neutralization was used. Pressure in the analytical chamber during spectral acquisition was about 5×10^{-9} Torr. Pass energy for survey spectra (composition) was 150 eV. Data analysis was carried out using the Service Physics ESCA 2000 A analysis program (Service Physics, Bend OR). The take-off angle (the angle between the sample normal and the input axis of the energy analyzer) was 55° (55° take-off angle ≅ 50 - 70Å sampling depth). To overcome the short penetration of the XPS signal, three measurements from various parts of the carbon materials, including fractured surfaces from inside the sample to represent the bulk composition, were acquired for each sample. The XPS atomic percentage was calculated using the area under each peak after the background was subtracted.

Table 2
BET data and specific capacitance measured at 1 mA.

Sample ID	S_BET	D _DA	C_g	C_g 10K	C_BET	C_BET 10K
HMTA	1063	1.48	93.9	84.9	0.081	0.071
YP17	1334	1.58	89.5	92.6	0.067	0.069
NaOH	589	1.52	30.1	22.6	0.051	0.038

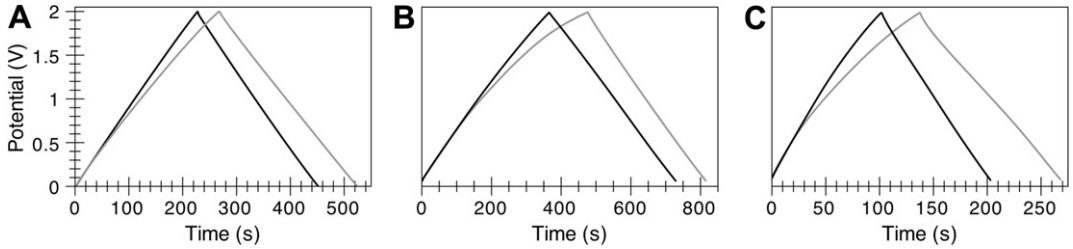

Fig. 3. Series of galvanic cycles measured at 1 mA for HMTA carbon (A), coconut-based sample YP17 (B), and carbon cryogel made with NaOH (C). The HMTA carbon in A has the characteristic straight slope of a double layer capacitor in both the charge and discharge cycles. B and C show non-linear behavior characteristic of faradaic reactions. The gray curve is the initial cycles and the black is after 10K cycles.

A linear baseline subtraction was used under each peak. The percentage was calculated using Eq. (1).

$$\text{Atomic}\,\% = \frac{\text{Area of the peak}}{\text{Sum of all peaks}} \times 100 \tag{1}$$

2.3. Electrochemical analysis

The electrodes were prepared by grinding monoliths into a fine powder then mixing with 3 wt% of polytetrafluoroethylene (PTFE). The resulting electrodes had a thickness of 0.08 mm and a diameter of 10 mm. To test the electrodes, a 2-electrode test cell was used with one of the carbon electrodes as the counter and reference electrode. A Celgard® porous film separated the electrodes, and to reduce the interfacial effect, specially coated aluminum contacts were used. The electrochemical test cell was assembled and sealed under an argon rich environment (ca. 70% Ar according to glove box manufacturer PlasLabs). To increase the penetration of the electrolyte into the pores the samples were wetted under a −0.1 MPa vacuum (process repeated three times). Tetraethylammonium tetrafluoroborate (TEATFB) in saturated 50/50 propylene carbonate/dimethylcarbonate was used as the electrolyte. The equations used to convert the electrochemical data are described elsewhere [16]. The specific quantities in terms of the BET surface area were calculated based on the specific gravimetric capacitance [17]. The specific capacitance based on the BET surface area, C_{BET}, was calculated using Eq. (2).

$$C_{BET} = \frac{C_g(F/g)}{SA_{BET}(m^2/g)} \tag{2}$$

where C_g is the gravimetric capacitance of a single electrode (F/g) and SA_{BET} is the gravimetric specific surface area of the electrode (m^2/g).

The electrochemical measurements, galvanic cycles (GC), and electrochemical impedance spectroscopy were performed with a Solartron 1287A using a voltage range between 0 and 2 V. The GC was measured at 0.5, 1, 5, 10, 50 and 100 mA. Electrochemical impedance spectroscopy was done using the Solartron 1287A in conjunction with a Solartron 1260 FRA/impedance analyzer; the samples were cycled and pretreated at +2 V prior to measurements. An AC voltage amplitude of 10 mV and a frequency range of 0.1 MHz−1 mHz was used for the scan. After the impedance analysis, the samples were cycled at a current of 40 mA for 10,000 cycles to test the endurance of the capacitors. The GC's and the impedance analysis were repeated after the cycles concluded.

3. Results and discussion

3.1. Chemical composition structure and performance

The XPS spectra in Fig. 1 show the differences between the carbon electrodes catalyzed using hexamine (HMTA), and those using coconut shells (YP17), and catalyzed using NaOH. As seen in Fig. 1 A, the main impurity in the hexamine catalyzed sample was oxygen, with a binding energy of ca. 533 eV. On the other hand, the coconut and NaOH catalyzed samples had much higher concentrations of oxygen, between 8 and 17%, with the oxygen's binding energy ca. 531eV. The percent of impurities measured by XPS is summarized in Table 1.

Since the three carbon samples came from different sources, it was expected for the microstructures to differ as seen in Fig. 2. The BET data, summarized in Table 2, show only the total BET surface area and the micropore diameter since these values are the ones to affect the capacitance of the device. The surface area increases the charge storage and the pore size limits the power losses and the capacitor relaxation [16]. However the BET surface area can be used as a normalization factor to both evaluate the capacitance and losses of the device and the impact of the impurities as faradaic reactions [17]. Note that the micropore diameter in Table 2 is comparable for all the samples and close to the mesopore limit of 2 nm. Therefore the capacitor's pore size should not limit the penetration of the electrolyte [16]. In Table 2, the gravimetric

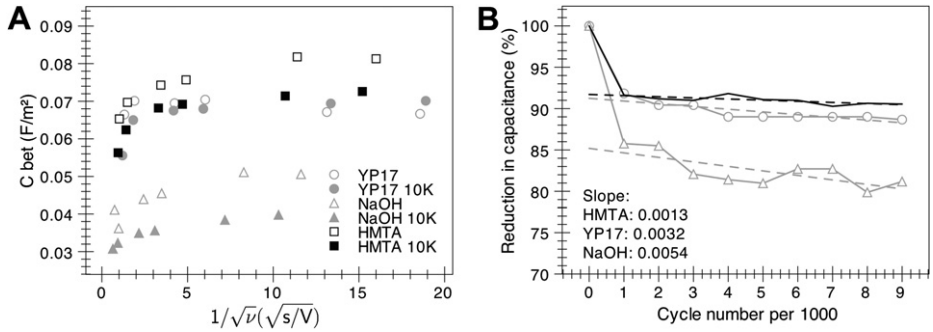

Fig. 4. Capacitance per unit surface area as a function of voltage rate (A) and percent of capacitance reduced during cycling at 40 mA (B).

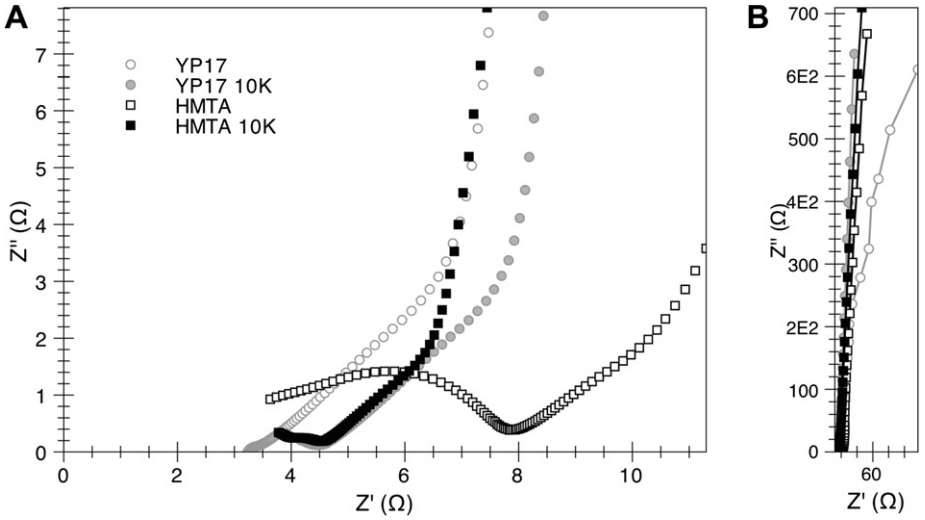

Fig. 5. ESR (A) and low frequency impedance data (B). The faradaic reactions from YP17 can be seen in the sample prior to cycling in the low frequency data. After cycling, the capacitor behaves more like a double layer capacitor. The HMTA sample does not have this faradaic effect and the resistance is greatly reduced after cycling.

capacitance of the supercapacitors measured at 1 mA and the capacitance per BET surface area were compared before and after cycling. Note that although the HMTA catalyzed electrodes and the commercial coconut shell carbons had similar capacitances, the capacitance normalized using the BET surface area decreased with the addition of impurities, in this case oxygen. In the samples used, the capacitance per BET surface area decreased from 0.08 in the HMTA case to 0.03 F/m^2 in the NaOH case. Although these types of measurements are widely used to evaluate supercapacitors, the rate of charge and discharge and a more in-depth frequency dependence study can provide mechanisms for how these impurities affect the device.

3.2. Cycle stability

Faradaic reactions affected the charge–discharge rate when impurities were present in the capacitor [4,5]. In Fig. 3A, the galvanic cycles at 1 mA for the HMTA electrodes was almost perfectly linear, expected of an electric double layer capacitor. This linear behavior remained even after 10,000 cycles. The rate of charge is 9 mV/s at the beginning and ca. 7.5 at the end of 10,000 cycles. In Fig. 3B and C, the faradaic reactions were evident from the non-linear charge and discharge cycles. In Fig. 3B, at the beginning YP17 had an asymmetric charge–discharge cycle with voltage rate $\nu = 4$ and -6 mV/s, respectively. The linear discharge of YP17 can be attributed to a charge selective faradaic reaction, in this case from the oxygen containing functional groups in the YP17 carbon under the chosen voltage range. The faradaic component in YP17 decreased after the 10K cycles, behaving like an EDL capacitor. The charge and discharge became symmetric (ν] = 5 and -5 mV/s, respectively). However in Fig. 3C, showing the sample produced under laboratory conditions using NaOH, both charge and discharge cycles presented aspects characteristic of faradaic reactions that diminished after the 10K cycles. But contrary to the YP17 sample, the charge–discharge curves are symmetric like those seen in a reversible process ($\nu = 14$ and -14 mV/s). The reversible process was likely due to the Na+ and OH- ions from the sodium hydroxide left in the carbon. The galvanic cycles demonstrate that the three samples have very distinct attributes regarding the formation of the electric double layer and the presence of pseudocapacitance.

Fig. 4A shows the capacitance as a function of $1/\sqrt{\nu}$. The penetration of the electrolyte molecules at lower voltage rate (high $1/\sqrt{\nu}$) was affected by the 10K cycling at 40 mA. Moreover, while not highly notable in the gravimetric capacitance (see Table 2), the specific capacitance per unit surface area shows a reduction of the charge storage from the HMTA electrodes to the YP17 and NaOH ones. The HMTA sample has a maximum capacitance of ca. 0.08 F/m^2 and even after cycling, the capacitance stayed slightly above that of the commercial sample YP17. The HMTA and NaOH samples show a marked decrease after the 10,000 cycles not seen in YP17. This absence in the reduction can be attributed to the oxygen induced pseudocapacitive reaction occurring in YP17 that initially reduced the discharge capacitance and later restored it once the reaction was no longer present. In the case of the HMTA and NaOH catalyzed

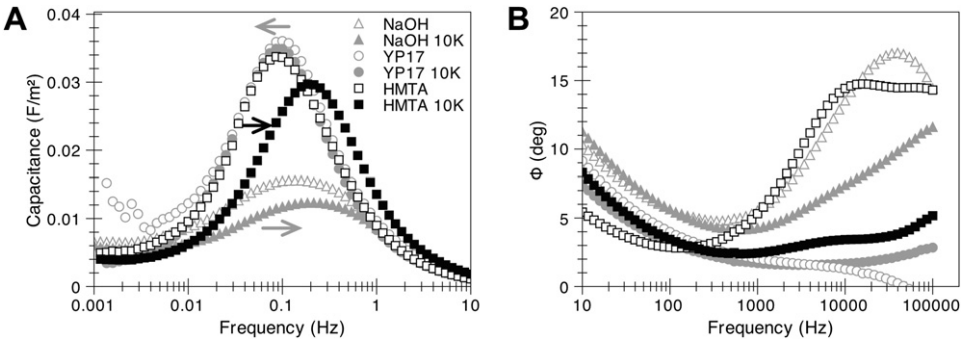

Fig. 6. Low frequency energy losses from the complex capacitance (A) and high frequency energy loss from the phase angle (B).

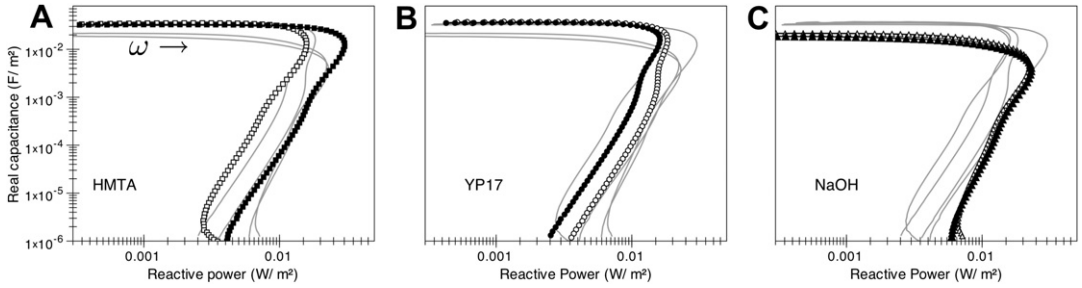

Fig. 7. Real capacitance vs. reactive power for HMTA catalyzed (A), coconut YP17 (B), and NaOH catalyzed (C) samples. The plots of the corresponding samples are highlighted over those of the other samples for ease of comparison.

samples, the charge decreased after cycling, likely from their reversible nature. For the HMTA sample, the reduction in capacitance can be attributed to various aging mechanisms [5] common in EDLSC.

During cycling at 40 mA, the capacitance loss can be seen in Fig. 4B. The HMTA and YP17 samples have only a 10% loss of the capacitance during the first 10 K cycles, while a loss of 20% is seen in the NaOH sample. However, if the rate of capacitance loss is calculated, the HMTA sample has a cycle life that doubles that of YP17 and NaOH (based on the slope of the capacitance loss of HMTA, YP17, and NaOH. See Fig. 4B). Note that these capacitors are not prepared under ideal conditions: a 100% inert atmosphere is required to extend the life of the electrolyte at the high voltages used. However, the HMTA carbon has a performance that can exceed that of the commercial carbons without the aid of faradaic reactions.

3.3. Interpretation using EIS

The galvanostatic measurements do not provide discrete information on the role some of the faradaic reactions have on the supercapacitor as a device. Supercapacitors are energy and power devices [2]; energy and power can be from that delivered or stored by the device or that lost due to an irreversible process [16]. To best describe their performance, impedance spectroscopy allows for the separation of these processes in the device.

The impedance spectra of the supercapacitors show how the pure carbon HMTA compares to the commercial sample YP17. The NaOH sample was not included since not much variation was observed from this plot. At the high frequency range of the spectra, the HMTA sample had a large equivalent series resistance (ESR) prior to the repetitive cycling. This resistance was over 6 times greater than that of the YP17 sample. However after 10 K cycles, the resistances of both samples YP17 and HMTA are almost indistinguishable. The reduction of the ESR in HMTA was enhanced by increased penetration of the electrolyte ions within the porous network. However, the YP17 increased its ESR. This increase can be attributed to the consumption of the oxygen faradaic contribution that originally decreased its ESR. The faradaic reaction developed in the low frequency impedance spectra shown in Fig. 5 B. While the HMTA sample has a linear, almost perpendicular, spectra characteristic of electric double layer supercapacitors before and after cycling (squares in Fig. 5B), the YP17 sample forms an arch (open circles in Fig. 5B) indicative of faradaic reactions. After repeated cycling this faradaic component disappears (closed circles in Fig. 5B).

The energy losses attributed to the impedance spectra can be seen while using the complex capacitance and the phase angle See Fig. 6A and B. At low frequencies of the spectra Fig. 6A, the relaxation of the capacitor is also affected by the presence of the impurities. The YP17 sample seems to have little change in its relaxation time τ and capacitance likely due to the charges produced by the oxygen impurities. After cycling, the HMTA sample and the NaOH sample have a gain in the relaxation time or have faster relaxations compared to the YP17 sample. This is also true of the losses produced by the interfacial effect at the high frequency range, Fig. 6B. On the other hand, cycling of the YP17 capacitor increased such losses.

The complex capacitance and complex power were used to separate the role of the energy and power produced by the capacitor. The complex power $Q(\omega)$ can be expressed in term of the real capacitance as shown in the equation $Q(\omega) = -\omega C'(\omega)|\Delta V_{rms}|$. The relation provides a plot similar to a Ragone plot. In Fig. 7, the real capacitance $C'(\omega)$, proportional to the total energy of the capacitor, is plotted against the reactive power $Q(\omega)$. Fig. 7A shows that the HMTA sample's capacitance is nearly unchanged, but due to the electrolyte's penetration, the reactive power is highly increased after 10 K cycles (dark squares). This is particularly important in applications where high power and energy are required. Although the commercial sample YP17 has good performance like HMTA, it has a loss in the reactive power as seen in Fig. 7B. This is likely due to the expenditure of the oxygen through faradaic reactions. In Fig. 7C, the NaOH sample retained a high power, however it came at a loss of the specific capacitance and energy. The reactive power, discharged by the capacitor, can be greatly improved by using pure carbons such as the HMTA catalyzed resin.

4. Conclusion

High purity carbons can be synthesized from renewable sources to produce electrodes for supercapacitors and other energy storage applications. The resorcinol-furfural cryogels catalyzed using hexametylenetetramine are not only good precursors for high surface area carbons with tunable structure, but also their purity can maximize the performance of supercapacitors like those that use organic electrolytes requiring carbon's inert properties. The results demonstrate that the capacitance per surface area can be increased 18% over that of the commercial sample (ca. 0.08 F/m^2) without the use of faradaic reactions. The lifetime of the device was also greatly improved with a cycle life twice that of the commercial sample. Another important aspect was the increase of the reactive power with cycling of the device due to increased penetration of the electrolyte.

Although the search for low-cost precursors has driven the use of these readily available biomass sources, there is also a need to provide high quality carbons for high performance applications. The resorcinol furaldehyde system described here can offer solutions to provide an all-renewable synthesis, which allows excellent performance by promoting double layer formation.

Acknowledgements

This work is supported in part by National Science Foundation (DMR-0605159 and CMMI-1030048). This research is also

supported by Washington Research Foundation, National Center for Nanomaterials Technology (Korea), Intel Corporation, and Pacific Northwest National Lab (PNNL). Betzaida Batalla Garcia and Stephanie L. Candelaria would like to acknowledge the NSF Bioenrgy IGERT (DGE-0654252).

References

[1] Hall PJ, Mirzaeian M, Fletcher Isobel S, Sillars FB, Rennie AJR, Shitta-Bey GO, et al. Energy storage in electrochemical capacitors: designing functional materials to improve performance. Energy Environ Sci 2010;3(9):1238.
[2] Burke AF. Batteries and ultracapacitors for electric, hybrid, and fuel cell vehicles. Proc IEEE 2007;95(4):806.
[3] Raymundo-Pinero E, Cadek M, Beguin F. Tuning carbon materials for supercapacitors by direct pyrolysis of seaweeds. Adv Funct Mater 2009;19(7):1032.
[4] Rufford TE, Hulicova-Jurcakova D, Zhu Z, Lu GQ. Nanoporous carbon electrode from waste coffee beans for high performance supercapacitors. Electrochem Commun 2008;10(10):1594–7.
[5] Andreas HA, Lussier K, Oickle AM. Effect of Fe-contamination on rate of self-discharge in carbon-based aqueous electrochemical capacitors. J Power Sources 2009;187(1):275–83. Sp. Iss. SI.
[6] Azais P, Duclaux L, Florian P, Massiot D, Lillo-Rodenas MA, Linares-Solano A, et al. Causes of supercapacitors ageing in organic electrolyte. J Power Sources 2007;171(2):1046–53.
[7] Sricharoenchaikul V, Pechyen C, Aht-ong D, Atong D. Preparation and characterization of activated carbon from the pyrolysis of physic nut (Jatropha curcas L.) waste. Energy Fuels 2008;22(1):31–7.
[8] Wu D, Fu R, Zhang S, Dresselhaus M, Dresselhaus G. The preparation of carbon aerogels based upon the gelation of resorcinol-furfural in isopropanol with organic base catalyst. J Non-Cryst Solids 2004;336(1):26.
[9] Tian HY, Buckley CE, Mule S, Paskevicius M, Dhal BB. Preparation, microstructure and hydrogen sorption properties of nanoporous carbon aerogels under ambient drying. Nanotechnology 2008;19(47).
[10] Garcia BB, Liu D, Sepehri S, Candelaria SC, Beckham DM, Savage LW, et al. Hexamethylenetetramine multiple catalysis as a porosity and pore size modifier in carbon cryogels. J Non-Cryst Solids 2010;356(33–34):1620–5.
[11] White RJ, Budarin V, Luque R, Clark JH, Macquarrie DJ. Tuneable porous carbonaceous materials from renewable resources. Chem Soc Rev 2009;38(12):3401–18.
[12] Maeki-Arvela P, Holmbom B, Salmi T, Murzin DY. Recent progress in synthesis of fine and specialty chemicals from wood and other biomass by heterogeneous catalytic processes. Catal Rev - Sci Eng 2007;49(3):197–340.
[13] Ullmann F, Gerhartz W, Yamamoto YS, Campbell FT, Pfefferkorn R, Rounsaville JF. Ullmann's encyclopedia of industrial chemistry. 7th ed. Weinheim, Federal Republic of Germany/Deerfield Beach, FL, USA: VCH; 2007.
[14] Effendi A, Gerhauser H, Bridgwater AV. Production of renewable phenolic resins by thermochemical conversion of biomass: a review. Renew Sust Energ Rev 2008;12(8):2092–116.
[15] Reinout H, Sangwon S. The computational structure of life cycle assessment. Norwell, MA, USA: Kluwer Academics Publisher; 2002.
[16] Garcia BB, Feaver AM, Champion RD, Zhang Q, Fister TT, Nagle KP, et al. Effect of pore morphology on the electrochemical properties of electric double layer carbon cryogel supercapacitors. J Appl Phys 2008;104(1):014305.
[17] Sepehri S, Garcia BB, Zhang Q, Cao G. Enhanced electrochemical and structural properties of carbon cryogels by surface chemistry alteration with boron and nitrogen. Carbon 2009;47(6):1436.